Journal of Inflammation Research

Dovepress
Taylor & Francis Group

Open Access Full Text Article

ORIGINAL RESEARCH

Thyroid Stimulating Hormone May Facilitates Adipose Tissue Insulin Resistance by Inducing M1 Macrophage Polarization

Mengfei Fu*, Hanyu Wang*, Yuhan Zhang*, Liu Yang*, Yang Chen, Xiao Chen, Zixuan Wang, Hui Sun

Department of Endocrinology, Union Hospital, Tongji Medical College, Huazhong University of Science and Technology, Wuhan, People's Republic of China

*These authors contributed equally to this work

Correspondence: Hui Sun, Email sunny68@hust.edu.cn

Background: Recent studies suggest connection between the thyroid stimulating hormone (TSH) and insulin resistance (IR). Adipose tissue is one of insulin's target tissues. However, currently the regulatory mechanism of TSH on the adipose tissue is not fully investigated yet.

Methods: We constructed a subclinical hypothyroidism (SCH) mouse model induced by methimazole with elevated TSH levels and then observed its metabolic profile, adipose tissue IR, and the adipose tissue macrophages (ATMs) phenotype. In vitro, we treated RAW264.7 cells and bone marrow-derived macrophages (BMDM) to assess the effect of TSH on macrophage polarization and explore the specific underlying mechanisms.

Results: SCH mice exhibited a poorer metabolic profile and an advanced adipose tissue IR. Meanwhile, the number of M1 ATMs was increased in SCH mice adipose tissue. In vitro, TSH induced endoplasmic reticulum stress in macrophages, which activated the GRP78-ATF6-CHOP signaling pathway, and further promoted M1 macrophage polarization. 4-phenylbutyric acid (4-PBA), an endoplasmic reticulum stress inhibitor, corrected the polarization imbalance of ATMs in SCH mice adipose tissue and improved adipose tissue dysfunction and IR.

Conclusion: TSH activated endoplasmic reticulum stress in macrophages, which induced the polarization of ATMs toward a pro-inflammatory M1 phenotype and promotes adipose tissue IR. Our findings highlight the possible relationship of TSH with immunity and metabolism.

Keywords: thyroid stimulating hormone, adipose tissue macrophages, macrophage polarization, insulin resistance, inflammation

Introduction

Subclinical hypothyroidism (SCH) manifests as elevated serum thyroid stimulating hormone (TSH) levels along with normal free thyroxine (FT4) levels.[1] Multiple clinical studies have demonstrated the close association between SCH and the occurrence of insulin resistance, metabolic syndrome, and cardiovascular events.[2–4] Researchers have increasingly emphasized the clinical significance of TSH as one of the key parameters of thyroid function in SCH patients. Insulin resistance (IR) is a pathological condition in which target tissues such as adipose tissue, liver, and skeletal muscle have impaired insulin sensitivity or responsiveness,[5] is characterized by a chronic low-grade inflammatory state in the body which persists over time.[6,7] Scholars have investigated the specific mechanisms by which TSH acts on different insulin target tissues, such as the liver and skeletal muscle, to cause IR or improve insulin sensitivity.[8–10] Adipose tissue is crucial for in vivo glucose homeostasis regulation. However, the regulatory mechanism of TSH on the adipose tissue is not fully investigated yet.

Adipose tissue plays an important role not only in energy storage and balance, but also in metabolic processes, as it is an endocrine organ that secretes various bioactive substances.[11–13] Furthermore, adipose tissue is a large immunologically active organ and displays hallmarks of both and innate and adaptive immune response.[14,15] It is not difficult to see that adipose tissue has both metabolic and immunological activity.

Received: 11 February 2025
Accepted: 14 June 2025
Published: 25 June 2025

Graphical Abstract

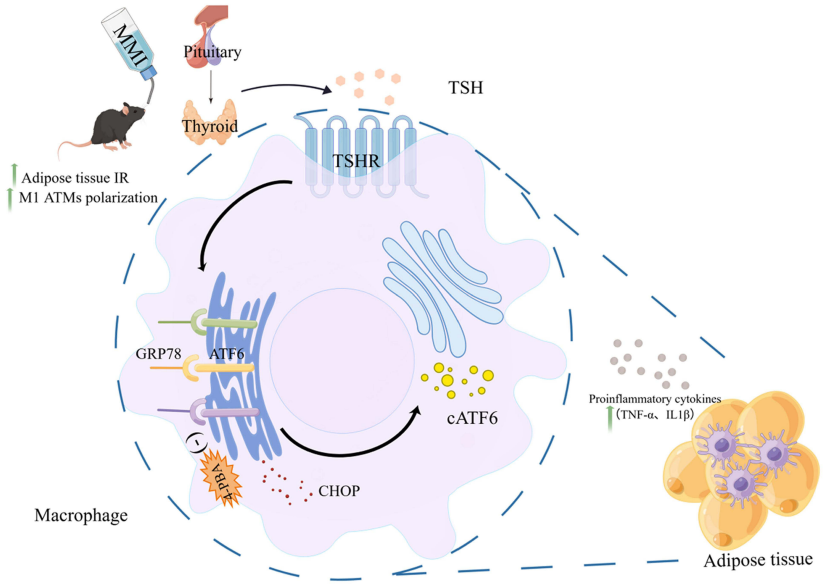

In methimazole(MMI) -induced subclinical hypothyroidism (SCH) mice, elevated thyroid stimulating hormone (TSH) stimulated adipose tissue macrophages (ATMs) via TSH receptor (TSHR), inducing endoplasmic reticulum stress through GRP78-ATF6-CHOP signaling. This drove M1 polarization and increased pro-inflammatory cytokines, resulting in adipose tissue insulin resistance (IR).

Adipose tissue macrophages (ATMs) are the largest proportion of immune cells in adipose tissue and are involved in various physiological regulatory processes (such as insulin sensitivity and tissue remodeling). ATMs are critical mediators in the onset and progression of adipose tissue inflammation and IR, as well as important in the immunity and the metabolism.[16] Furthermore, ATMs are heterogeneous and plastic, implying that their phenotype could change in response to alterations in the local microenvironment. The different phenotypes of macrophages are key contributor in the progression and regression of inflammation.[17] Increased infiltration of macrophage in adipose tissue, activation of pro-inflammatory phenotype (M1 macrophages), and production of proinflammatory cytokines, such as tumor necrosis factor- α (TNF-α), interleukin (IL)1β, and IL6, result in a vicious cycle of adipose tissue inflammation.[18]

ATMs are recognized as key players in the development of adipose tissue inflammation and IR, and in immune regulation.[19–22] Herein, based on the plasticity of the ATMs phenotype, we aim to investigate the role of ATMs as a bridge to study the regulatory mechanism of TSH on adipose tissue IR. We hypothesized that elevated TSH promotes M1 macrophage polarization, thereby impairing adipose tissue insulin sensitivity.

Materials and Methods

Animal Study

Male seven-week-old C57BL/6J mice were purchased from Beijing Vital River Company and housed in specific pathogen free (SPF) conditions at a temperature of 23±2°C and a humidity of 60%±10%. The animals were kept in 12 h alternate light and dark cycles to maintain a day and night pattern. All experimental protocols were approved by the Institutional Animal Care and Use Committee of Huazhong University of Science and Technology (No. 3600) and conducted in strict accordance with the Chinese National Standard "Guidelines for Ethical Review of Laboratory Animal Welfare" (GB/T 35892–2018).

After one week of acclimatization, the mice were randomly divided into two groups: Control (given normal drinking water) and SCH (given drinking water supplemented with methimazole (MMI), a drug that inhibits thyroid hormone

synthesis at a dose of 0.08 mg/kg d for 12 weeks). The mice were fed a normal diet throughout the study. As mentioned in previous studies,[23,24] the MMI (CatNo.301507, Sigma) dose was adjusted according to the animals' water intake and body weight. 4-phenylbutyric acid (4-PBA) (CatNo. S3592, Selleck), an endoplasmic reticulum stress (ERS) inhibitor, was injected into the mice at a dose of 100 mg/kg□d for 4 weeks after successfully constructing the SCH mouse model to clarify the role of ERS in vivo.

Intraperitoneal Glucose Tolerance Test (IPGTT) and Intraperitoneal Insulin Tolerance Test (IPITT)

The mice were intraperitoneally injected with 2 g/kg glucose after 16 h of fasting or 0.75 U/kg insulin after 4 h of fasting, and blood glucose was measured at 0, 30, 60, 90, and 120 min post-injection. The area under the curve (AUC) was then determined.

Serum Analysis

Alanine aminotransferase (ALT), aspartate aminotransferase (AST), total cholesterol (TC), triglyceride (TG), low-density lipoprotein (LDL), fasting serum glucose, glycated serum protein (GSP) were detected using an automatic biochemical analyzer (Biobase, Shan Dong, China). Non-esterified fatty acids (NEFA) were detected using the colorimetric assay kit (CatNo. A042-1-1, Nanjing Jiancheng Bioengineering Institute, Nanjing, China).

Enzyme Linked Immunosorbent Assay (ELISA)

Concentrations of free triiodothyronine (FT3) (CatNo. MU30578), FT4 (CatNo. MU30579), TSH (CatNo. MU30680), TNF-α (CatNo. MU30030), IL1β (CatNo. MU30369), IL6 (CatNo. MU30044), insulin (CatNo. MU30432), leptin (CatNo. MU30381), and adiponectin (ADPN) (CatNo. MU306297) were determined using specific ELISA kits (Bioswamp).

Histological Analysis and Immunohistochemistry

The animals' inguinal white adipose tissue (iWAT) and epididymal white adipose tissue (eWAT) were isolated, fixed in an AT fixative, paraffin-embedded, and later cut into 5 μm sections. Staining was performed with hematoxylin and eosin (HE) or by immunohistochemistry (IHC).

Isolation of Bone Marrow-Derived Macrophages (BMDM)

In male six-week-old C57BL/6J mice, femur and tibiofibula, as well as surface hair and muscle, were removed, and the bone marrow cavity was flushed with RPMI 1640 medium (CatNo. PM150110, Procell) supplemented with 10% fetal bovine serum (CatNo. FBS500-A, HY Cezmbio) and 1% penicillin-streptomycin (CatNo. BL505A, Biosharp). Subsequently, 30 ng/mL granulocyte-macrophage colony-stimulating factor (CatNo. 315–03, Peprotech) was added to stimulate the bone marrow cells for seven days to extract BMDM.[25]

Isolation of SVF

Adipose tissue was minced in Hanks' balanced salt solution (CatNo. BL559A, Biosharp) containing calcium, magnesium, and 0.5% bovine serum albumin, digested with 1 mg/mL collagenase type II (CatNo. C6885, Sigma), and incubated at 37°C for 20~45 min with vigorous hand shaking every 10 min. The sample was then filtered through a 100 μm nylon filter and centrifuged at 500×g for 10 min. The white upper layer comprised adipocytes, while SVF was the lower precipitate.

Cell Culture

RAW264.7 cells (Wahlner Bio, Wuhan, China) were cultured in DMEM high glucose medium (CatNo. HYG4515, HY Cezmbio) supplemented with 10% fetal bovine serum (CatNo. FBS500-A, HY Cezmbio) and 1% penicillin-streptomycin (CatNo. BL505A, Biosharp Biosharp). And they were treated with 5ng/mL rmTSH for 48h (CatNo.8885-TH-010, R&D Systems),or 10μmol/l 4-PBA (CatNo. S3592, Selleck) for 12h, or DMSO (CatNo. D2605, Sigma) for 12h.

Flow Cytometry

Cell suspensions were collected into flow tubes and stained using antibodies against CD45(1:200, CatNo. 550994), F4/80 (1:200, CatNo. 565410), CD11b(1:200, CatNo. 557396), CD11c(1:200, CatNo. 558079), and CD206(1:200, CatNo. 565250), all purchased from BD Pharmingen. Subsequently, detection was performed using a BD LSR flow cytometer (BD Biosciences, San Jose, CA, USA), and data were analyzed using Flow Jo or CytExpert software.

Western Blot (WB)

Harvested tissues and cells were lysed in a RIPA lysate containing 1% protease and phosphorylated protease inhibitors (CatNo. P003, NCM Biotech). Protein concentration was determined using the BCA protein assay reagent (CatNo. P0010, Beyotime), and then 30 μg protein was added to each well, after which the proteins were transferred to a polyvinylidene fluoride membrane for closure. Following that, the membrane was incubated overnight with antibodies against GRP78(1:6000, CatNo.11587-1-AP), ATF6(1:8000, CatNo.24169-1-AP), CHOP(1:3000, CatNo.66741-1-Ig), p-Akt(1:1000, CatNo. 4060,CST), and Akt(1:6000, CatNo.10176-2-AP). Bands were detected using HRP-coupled anti-rabbit or anti-mouse IgG antibody (1:3000) and an ECL system. Almost all antibodies were obtained from the Proteintech Group, Inc. Protein band intensities were quantitatively analyzed using Image J software.

Quantitative Real-Time PCR (qPCR)

The total RNA extraction reagent (CatNo. BS258A, Biosharp) was employed to extract RNA from cells or tissues, which was then solubilized using DEPC-treated water. After determining RNA concentration, RNA mass was quantified to be 1,000 ng. Subsequently, cDNA was synthesized using the reverse transcription reagent (CatNo. R223-01,Vazyme) and primers (Tsingke Biotechnology), and then quantitatively analyzed using a real-time fluorescence quantification system. We used GAPDH as an internal control. The relative level of each target gene was calculated using the $2^{-\Delta\Delta Ct}$ method. Table 1 shows all the primer sequences used herein.

Immunofluorescence Staining

Cells were fixed in 4% paraformaldehyde, permeabilized with 0.5% Triton X-100 diluted in PBS, and then blocked with goat serum. They were then incubated overnight at 4°C with primary antibodies against GRP78(1:300), ATF6(1:100), and CHOP (1:200). The following day, the cells were washed 3 times and were incubated with Cy3-conjugated anti-mouse or anti-rabbit IgG antibody before adding the anti-fluorescence quencher. Notably, DAPI was used as a nuclear stain. A confocal microscope (Olympus BX51, Tokyo, Japan) was used to capture images.

Apoptosis Analysis

We collected and stained RAW264.7 cells with annexin V and the propidium iodide solution in an apoptosis detection kit (CatNo. C1062S, Beyotime) for 10 min at room temperature under light protection, after which more Binding Buffer was

Table 1 Primer Sequences Used for qPCR

Genes	Forward Sequences (5′to 3′)	Reverse Sequences (5′ to 3′)
F4/80	CATCATGGCATACCTGTTCAC	GAATGGGAGCTAAGGTCAGTC
CD68	TGTTCAGCTCCAAGCCCAAA	ACTCGGGCTCTGATGTAGGT
iNOS	GCGCTCTAGTGAAGCAAAGC	AGTGAAATCCGATGTGGCCT
TNF-α	CTCAGCGAGGACAGCAAGG	AGGGACAGAACCTGCCTGG
CCL2	GCTGGAGCATCCACGTGTT	GCTGGTGAATGAGTAGCAGCA
COX2	GCGACATACTCAAGCAGGAGCA	AGTGGTAACCGCTCAGGTGTTG
GRP78	ACTTGGGGACCACCTATTCCT	ATCGCCAATCAGACGCTCC
ATF6	AGACACTACCAGCCCTTATGCC	GTAGAACAGGTTTAGTCACGGA
CHOP	CTGGAAGCCTGGTATGAGGAT	CAGGGTCAAGAGTAGTGAAGGT
GAPDH	CTTCATTGACCTCAACTACATGGTCTA	GATGACAAGCTTCCCATTCTCAG

added and mixed well to make a 500 μL cell suspension. Detection was then performed using BD FACS Caliber within 1 h, and the data were analyzed using CytExpert software.

Nitric Oxide (NO) Assay

We detected NO concentration in the cell supernatant per the instructions in the NO assay kit (CatNo. S0021, Beyotime).

Statistical Analysis

The experimental data were analyzed using Prism 8.0 software. All values were expressed as mean±SD. Student's *t*-test and analysis of variance (ANOVA) were used for comparisons between two groups and between more than two groups, respectively. Differences were considered statistically significant at $P < 0.05$.

Results

SCH Mice Exhibit a Relatively Poor Metabolic State

Serum FT3, FT4 and TSH levels were detected after 12 weeks of MMI treatment. According to the results, although serum FT3 and FT4 concentrations in the two mice groups were comparable, TSH levels were significantly higher in the MMI-treated group (Figure 1A). Since MMI may impair liver function, we examined the serum ALT and AST levels in the two mice groups and found no significant differences (Figure 1B).

To assess the metabolic status of the mice, we first compared their body weight and found that SCH mice were heavier. Additionally, we separated and weighed the white adipose tissue (WAT) of the two mice groups and found that the fat mass was higher in SCH mice (Figure 1C and D). Subsequently, we examined the metabolic indices of both mice

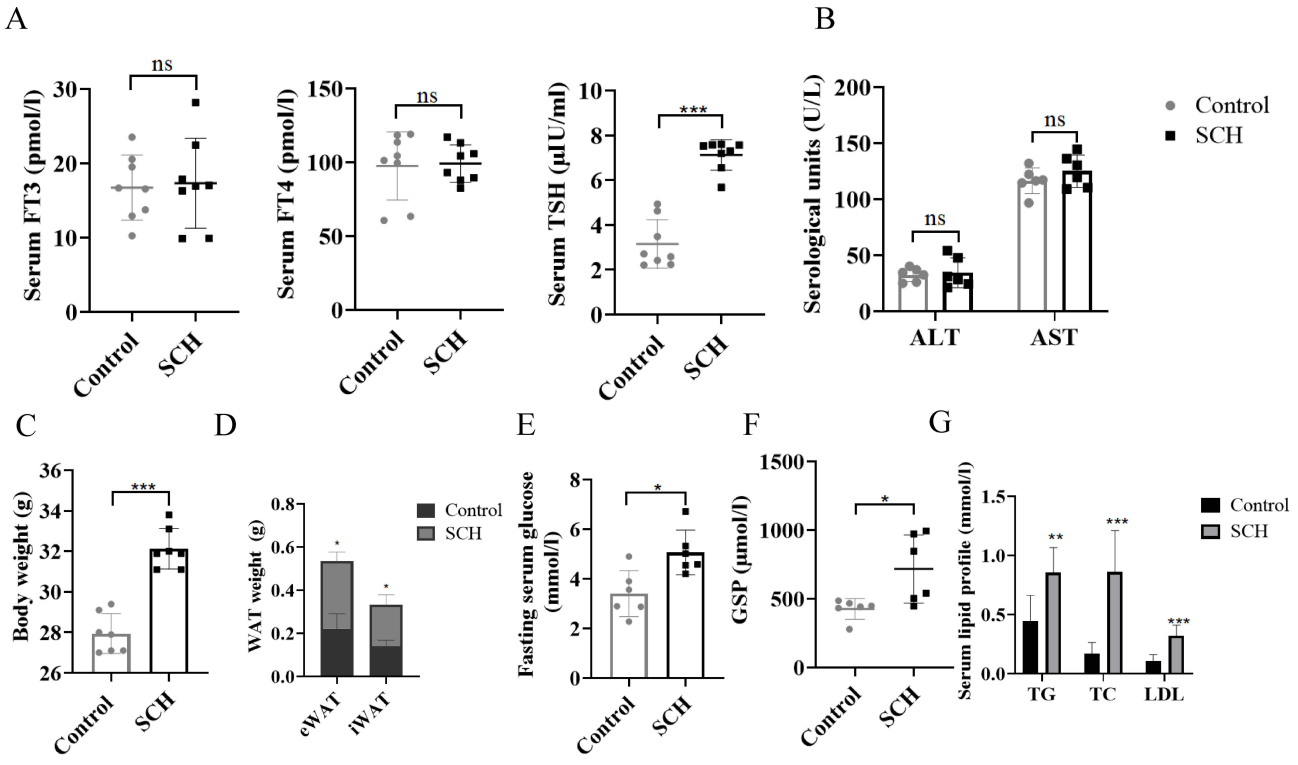

Figure 1 SCH mice exhibit a relatively poor metabolic state. (**A**) Serum concentration of FT3, FT4, and TSH. (**B**) Serum concentration of ALT and AST. (**C**) Body weights of control and SCH mice. (**D**) Weight of eWAT and iWAT. (**E**–**G**) Serum concentration of fasting serum glucose, GSP, and lipid profile. n=6–8. *P < 0.05, **P < 0.01, ***P<0.001 vs the Control group.

Abbreviations: ns, not significant; SCH, subclinical hypothyroidism; FT3, free triiodothyronine; FT4, free thyroxine; TSH, thyroid stimulating hormone; ALT, alanine aminotransferase; AST, aspartate aminotransferase; WAT, white adipose tissue; eWAT, epididymal white adipose tissue; iWAT, inguinal white adipose tissue; GSP, glycated serum protein; TG, triglyceride; TC, total cholesterol; LDL, low-density lipoprotein.

https://doi.org/10.2147/JIR.S522062

groups, including fasting plasma glucose, GSP, and serum lipid profile (TC, TG, and LDL), and discovered the presence of a relatively poor metabolic status in SCH mice (Figure 1E–G).

SCH Mice Have a More Advanced Insulin Resistance in Adipose Tissue

We first performed IPGTT to assess glucose homeostasis in mice. Compared to the control group, the blood glucose level was higher in SCH mice at 0, 30, and 60 min after being injected with glucose, implying their impaired glucose tolerance, a conclusion that was further supported by the AUC results (Figure 2A and B). We then performed IPITT to assess the insulin sensitivity of the mice. The results showed that insulin sensitivity was significantly reduced in SCH mice (Figure 2C and D). Furthermore, the homeostasis model assessment of insulin resistance (HOMA-IR) index further confirmed the increased IR in SCH mice (Figure 2E).

We aimed to assess the sensitivity of adipose tissue to insulin in this study, therefore, we calculated the adipose tissue insulin resistance (Adipo-IR) index by multiplying the fasting serum NEFA levels with insulin levels. As expected, SCH mice exhibited significantly elevated NEFA and insulin levels, as well as Adipo-IR index (Figure 2F and H). Additionally, the decreased levels of insulin-activated p-Akt in adipose tissue also confirmed the increased adipose tissue IR in SCH mice (Figure 2I and J).

SCH Mice Have More Severe Adipose Tissue Dysfunction

Adipocyte morphology is controlled by the metabolism.[26] In this state, adipocytes secrete various cytokines, recruit inflammatory cells, and initiate inflammatory programs, resulting in adipose tissue dysfunction.[27,28]

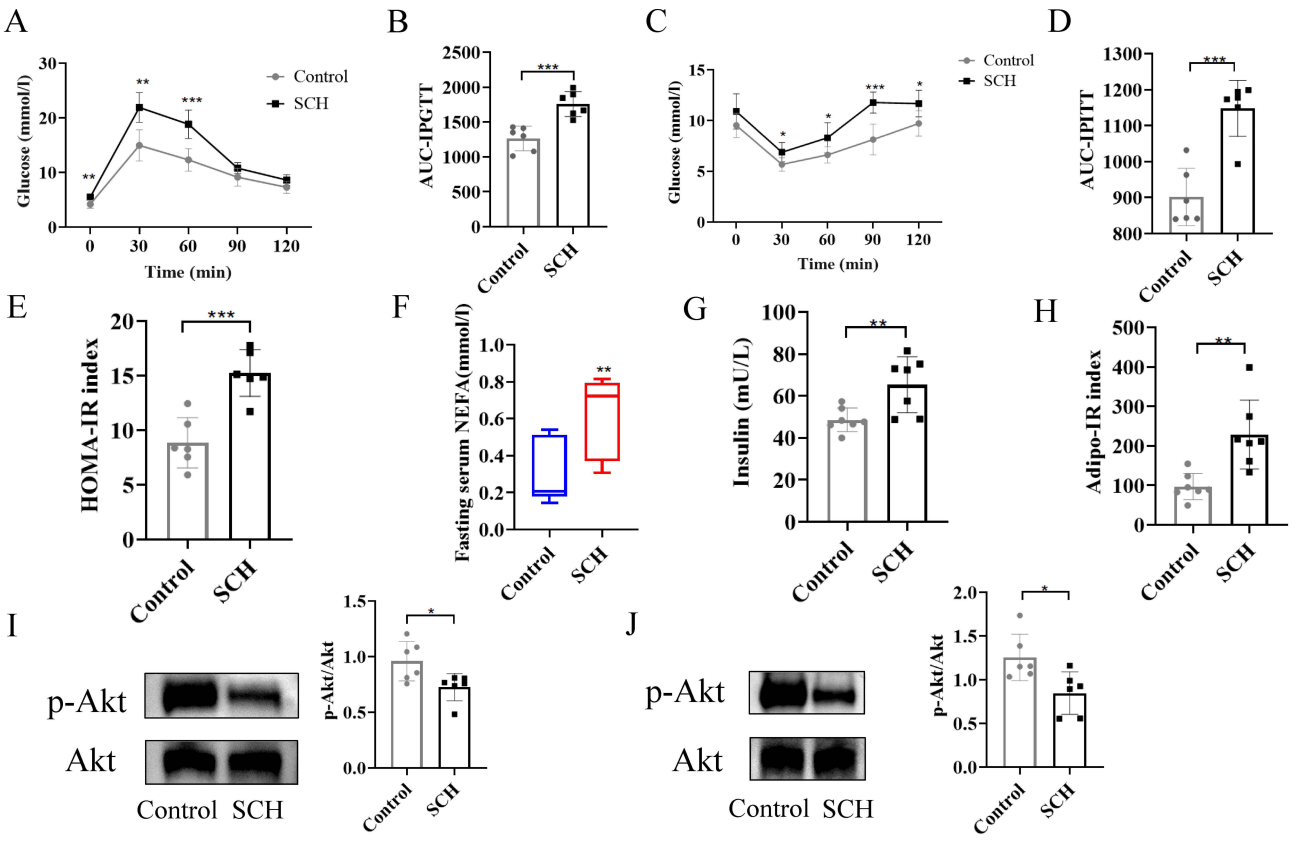

Figure 2 SCH mice have a more advanced insulin resistance in adipose tissue. (**A** and **B**) IPGTT and AUC of IPGTT. (**C** and **D**) IPITT and AUC of IPITT. (**E**) HOMA-IR index. (**F** and **G**) Fasting NEFA and insulin concentration. (**H**) Adipo-IR index. (**I** and **J**) The expression level of p-Akt/Akt proteins in eWAT (**I**) and iWAT (**J**) was determined by WB. n=6–7. *P < 0.05, **P < 0.01, ***P<0.001 vs the Control group.

Abbreviations: IPGTT, intraperitoneal glucose tolerance test; IPITT, intraperitoneal insulin tolerance test; AUC, area under the curve; HOMA-IR, homeostasis model assessment of insulin resistance; NEFA, non-esterified fatty acids; Adipo-IR, adipose tissue insulin resistance.

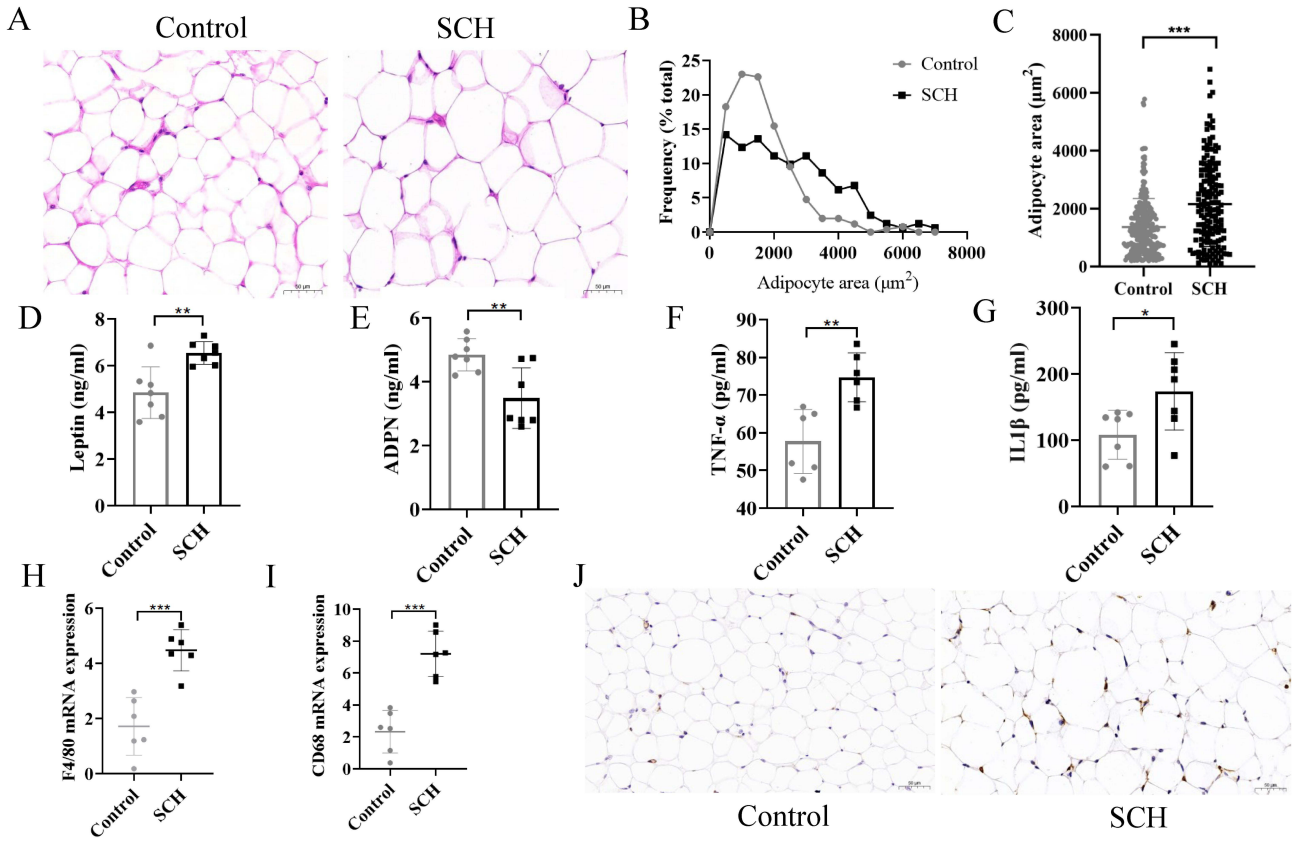

Figure 3 SCH mice have more severe adipose tissue dysfunction. (**A**) Representative HE staining images of eWAT (200×). Scale bars =50μm. (**B** and **C**) Manual analysis of adipocyte area in eWAT. (**D** and **E**) Serum concentrations of leptin and ADPN. (**F** and **G**) Serum concentrations of TNF-α and IL1β. (**H** and **I**) mRNA levels of F4/80 and CD68 in eWAT. (**J**) Representative F4/80 immunohistochemistry staining images of eWAT (200×). Scale bars=50μm. n=6–7. *P < 0.05, **P < 0.01, ***P<0.001 vs the Control group.
Abbreviations: ADPN, adiponectin; TNF-α, tumor necrosis factor-α; IL1β, interleukin 1β.

We observed significantly enlarged adipocytes in the eWAT of SCH mice (Figure 3A–C), and a similar phenomenon was observed in their iWAT (Figure S1A–C). Furthermore, SCH mice exhibited abnormal adipocytokine secretion, as evidenced by hyperleptinemia (Figure 3D), as well as significantly reduced ADPN levels (Figure 3E). We also detected significantly elevated serum levels of proinflammatory factors, such as TNF-α and IL1β, in SCH mice (Figure 3F and G). F4/80 and CD68 (two markers of ATMs) expression was significantly elevated in the adipose tissue of SCH mice (Figure 3H, I, Figure S1D and E). F4/80 immunohistochemistry, which also revealed increased macrophage infiltration in the adipose tissue of SCH mice (Figure 3J and Figure S1F).

The Number of M1 Macrophages Is Increased in the Adipose Tissue of SCH Mice

We examined the macrophage phenotype in the adipose tissue of the two groups of mice. The flow cytometry results showed a significant increase in CD11c-positive ATMs (Figure 4A and Figure S2A) and a significant decrease in CD206-positive ATMs (Figure 4B and Figure S2B) in the adipose tissue of SCH mice, findings that were further confirmed by IHC staining (Figure 4C, D, Figure S2C and D).

TSH Induces M1 Macrophage Polarization

Flow cytometry results showed a significant rise and decrease in the proportion of CD11c-positive macrophages (Figure 5A) and CD206-positive macrophages (Figure 5B), respectively, following TSH intervention. We then detected the concentration of pro-inflammatory factors such as TNF-α and IL6 in the cell culture supernatant by ELISA, confirming that TSH promoted the secretion of pro-inflammatory factors (Figure 5C and D). In addition, TSH also upregulated M1 macrophage markers, such as iNOS, TNF-α, and CCL2 (Figure 5E–G).

https://doi.org/10.2147/JIR.S522062

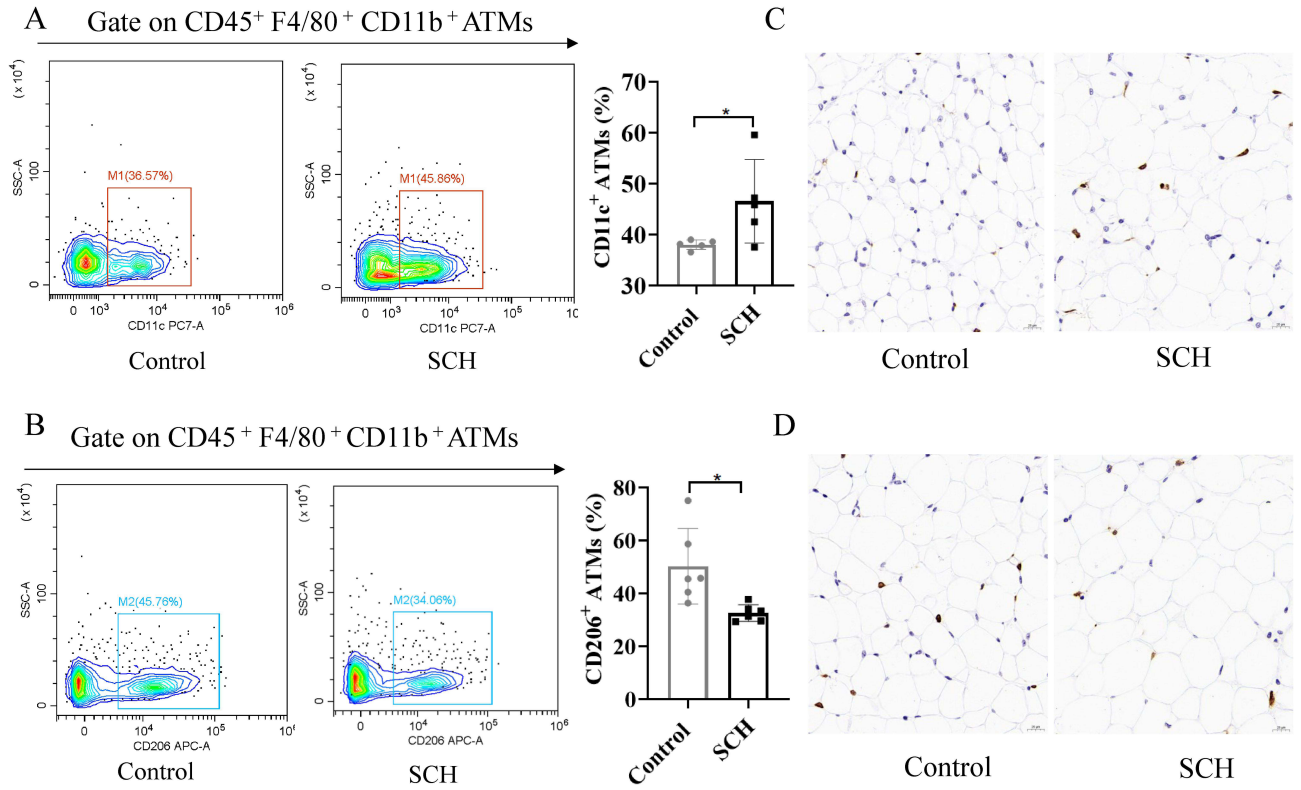

Figure 4 The number of M1 macrophages is increased in the adipose tissue of SCH mice. (**A**) The proportion of M1 (CD11c-positive) ATMs in eWAT. (**B**) The proportion of M2 (CD206-positive) ATMs in eWAT. (**C**) Representative CD11c immunohistochemistry staining images of eWAT (200×). Scale bars=20μm. (**D**) Representative CD206 immunohistochemistry staining images of eWAT (200×). Scale bars=20μm. n=5–6.*P < 0.05 vs the Control group.
Abbreviation: ATMs, adipose tissue macrophages.

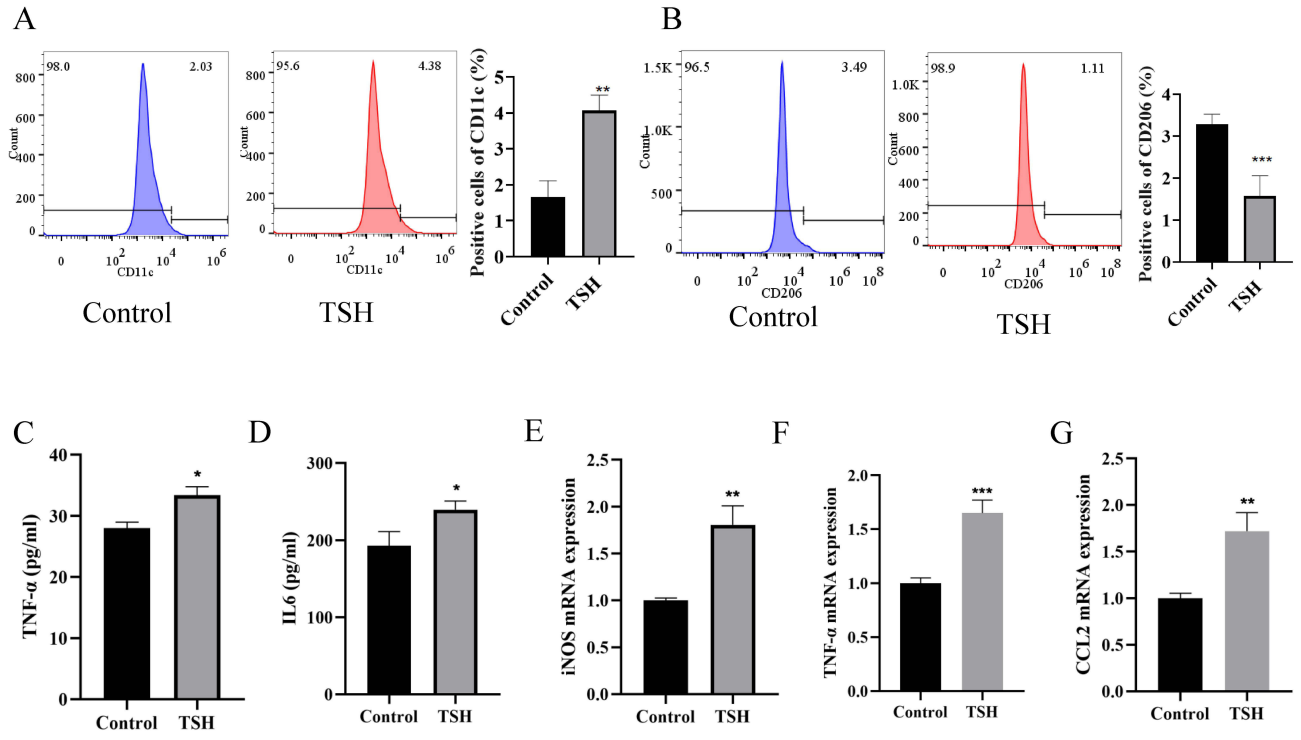

Figure 5 TSH induces M1 macrophage polarization. RAW264.7 cells were incubated with rmTSH (5ng/mL) for 48 h. (**A** and **B**) The proportion of M1(CD11c-positive) and M2 (CD206-positive) macrophages. (**C** and **D**) Concentration of TNF-α and IL6 in the cell culture supernatant. (**E**–**G**) mRNA levels of M1 macrophage markers (iNOS, TNF-α, CCL2). n=3.*P < 0.05, **P < 0.01, ***P<0.001 vs the Control group.
Abbreviation: TNF-α, tumor necrosis factor-α; IL6, interleukin 6; iNOS, inducible nitric oxide synthase; CCL2,chemokine (C-C motif) ligand 2.

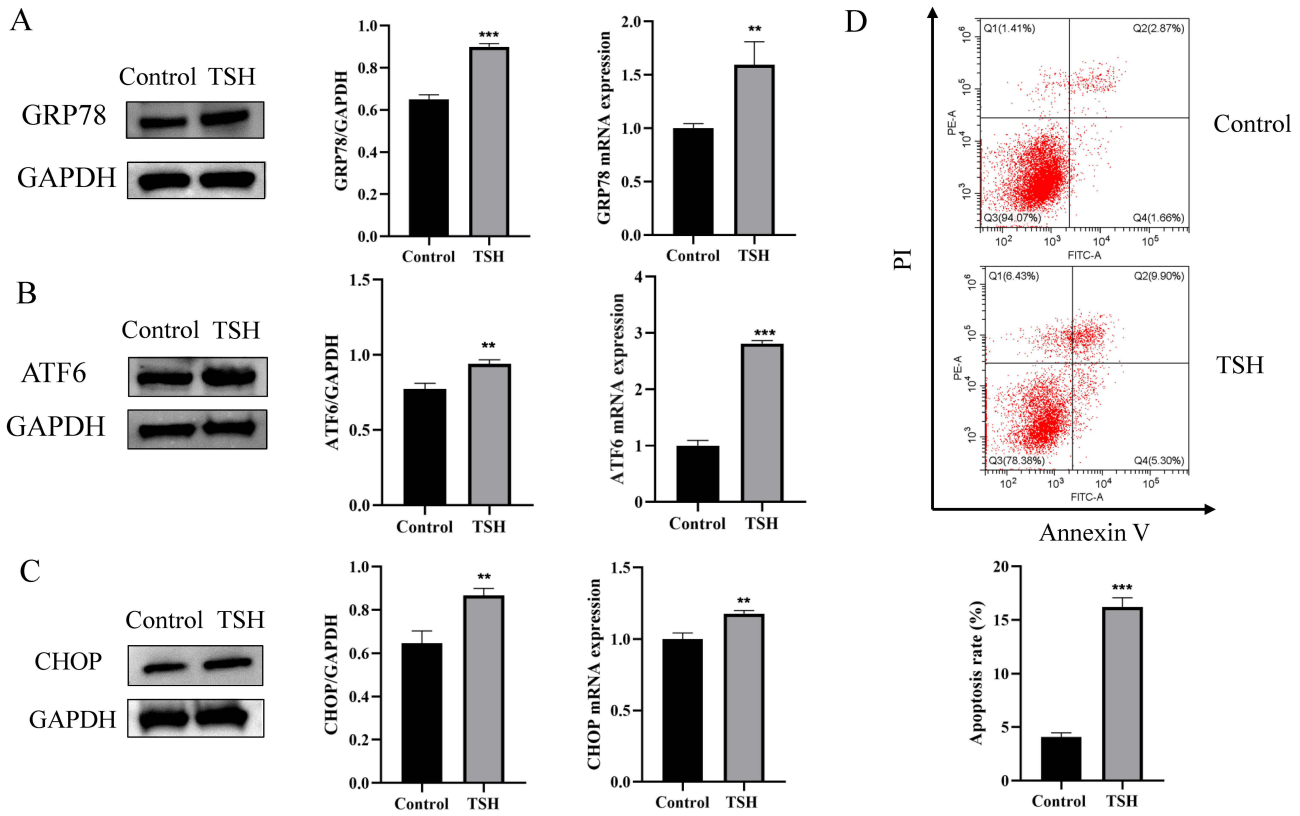

Figure 6 TSH induces endoplasmic reticulum stress in macrophages and activates the GRP78-ATF6-CHOP signaling pathway. RAW264.7 cells were incubated with rmTSH (5ng/mL) for 48 h. (**A**–**C**) Protein and mRNA expression levels of GRP78, ATF6, CHOP were detected by WB and qPCR, respectively. (**D**) Apoptosis rate. n=3. **P < 0.01, ***P<0.001 vs the Control group.

Abbreviations: GRP78, glucose-regulated protein 78; ATF6, activating transcription factor 6; CHOP, C/EBP-homologous protein.

TSH Induces Endoplasmic Reticulum Stress in Macrophages and Activates the GRP78-ATF6-CHOP Signaling Pathway

To elucidate the specific mechanism underlying TSH-induced M1 macrophage polarization, we focused on ERS. Both WB and qPCR confirmed that TSH intervention significantly increased the intracellular GRP78(an ERS marker) level (Figure 6A). Moreover, we further explored the downstream signaling pathways. We discovered that TSH upregulated ATF6 (Figure 6B), leading to a significant increase in CHOP expression (Figure 6C). The immunofluorescence images of BMDM also confirmed our conclusions (Figure S3). Given that CHOP is critically involved in ERS-mediated apoptosis, we analyzed the macrophage apoptosis rate and discovered that it rose after TSH intervention (Figure 6D).

TSH Promotes M1 Macrophage Polarization Through Endoplasmic Reticulum Stress

We sought to establish whether the TSH-induced ERS in macrophages could further lead to M1 macrophage polarization. In this regard, we treated RAW264.7 cells with 4-PBA (an ERS inhibitor) or an equal volume of DMSO, in regimens grouped as follows: Con+DMSO, Con+4-PBA, TSH+DMSO, and TSH+4-PBA. The proportion of CD11c-positive cells was significantly reduced after the addition of 4-PBA (TSH+4-PBA group vs TSH+DMSO group) (Figure 7A). The levels of M1 macrophage markers (iNOS, TNF-α, and COX2) were also decreased after ERS inhibition (Figure 7B–D). Similarly, 4-PBA reduced the levels of proinflammatory cytokines (Figure 7E–F) as well as NO (a major product of M1 macrophages) concentration (Figure 7G). Additionally, we validated the above results on BMDM (Figure S4A–C).

https://doi.org/10.2147/JIR.S522062

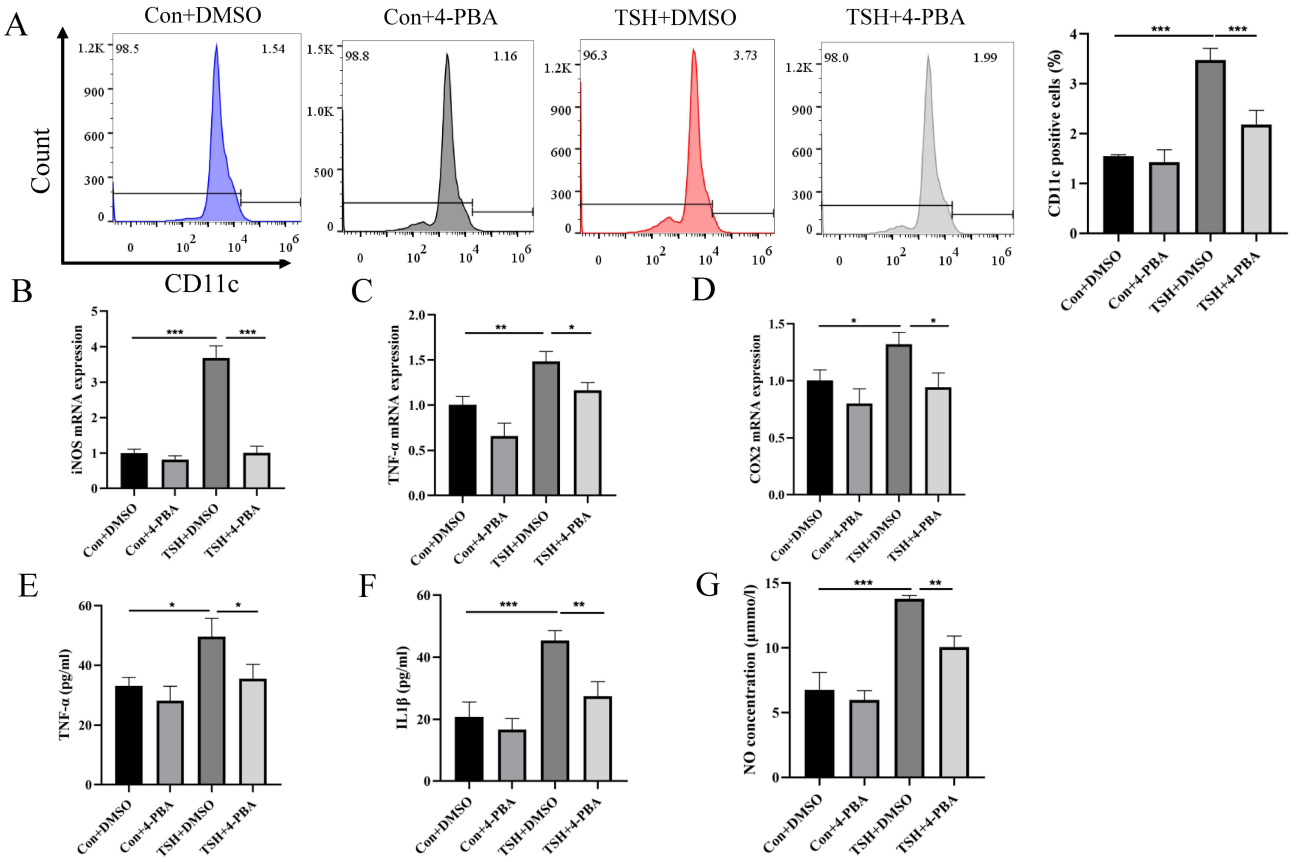

Figure 7 TSH promotes M1 macrophage polarization through endoplasmic reticulum stress. RAW264.7 cells were pretreated with 4-PBA (10μmol/l) or an equal volume of DMSO for 12 h and then incubated with rmTSH (5ng/mL) for 48 h. (**A**) Proportion of M1(CD11c-positive) macrophages. (**B**–**D**) mRNA levels of M1 macrophage markers (iNOS, TNF-α, COX2). (**E**–**G**) The concentration of TNF-α, IL1β and NO in the cell culture supernatant. n=3.*P < 0.05,**P < 0.01, ***P<0.001.
Abbreviations: iNOS, inducible nitric oxide synthase; TNF-α, tumor necrosis factor-α; COX2, cyclooxygenase 2; IL1β, interleukin1β; NO, nitric oxide.

Endoplasmic Reticulum Stress Mediates Adipose Tissue Insulin Resistance and M1 Macrophage Polarization in SCH Mice

To reduce GRP78 expression, mice were administered 4-PBA via intraperitoneal injection (Figures 8A, S5, S6 and S7A) and randomly divided into four groups: Con+Veh, Con+4-PBA, SCH+Veh, and SCH+4-PBA.

Intraperitoneal administration of 4-PBA in SCH mice significantly reduced the Adipo-IR index and increased p-Akt levels (Figure 8B, C, S7B). We then discovered that serum levels of leptin and proinflammatory factors (TNF-α and IL1β) were reduced in 4-PBA-treated SCH mice (Figure 8D–F), and as shown by F4/80 immunohistochemistry staining, macrophage infiltration in adipose tissue was also reduced (Figure 8G and Figure S7C). We also observed that 4-PBA downregulated M1 ATM markers, such as iNOS, TNF-α, and CCL2, in the adipose tissue of SCH mice (Figure 8H–J, S7D–F).

Discussion

It is well known that TSH is an anterior pituitary gland-secreted glycoprotein hormone comprising α- subunits and β-subunits bound by non-covalent bonds, and acts by binding to the thyroid stimulating hormone receptor(TSHR).[29] It has recently been discovered that TSH not only acts on thyroid follicular cells to regulate cell proliferation, as well as thyroid hormone synthesis and secretion, but also binds directly to the TSHR on the surface of extra-thyroidal tissues, such as liver and adipose tissue, and is involved in regulating the body's inflammation, as well as glucose and lipid metabolism.[9,30–33]

We constructed a SCH mouse model to investigate the role played by TSH in vivo. Since WAT involvement has been confirmed in various biological processes in vivo, including energy homeostasis, as well as glucose and lipid metabolism,[34,35] we explored WAT in SCH mice. In other words, we aimed to clarify the role of TSH in the regulation

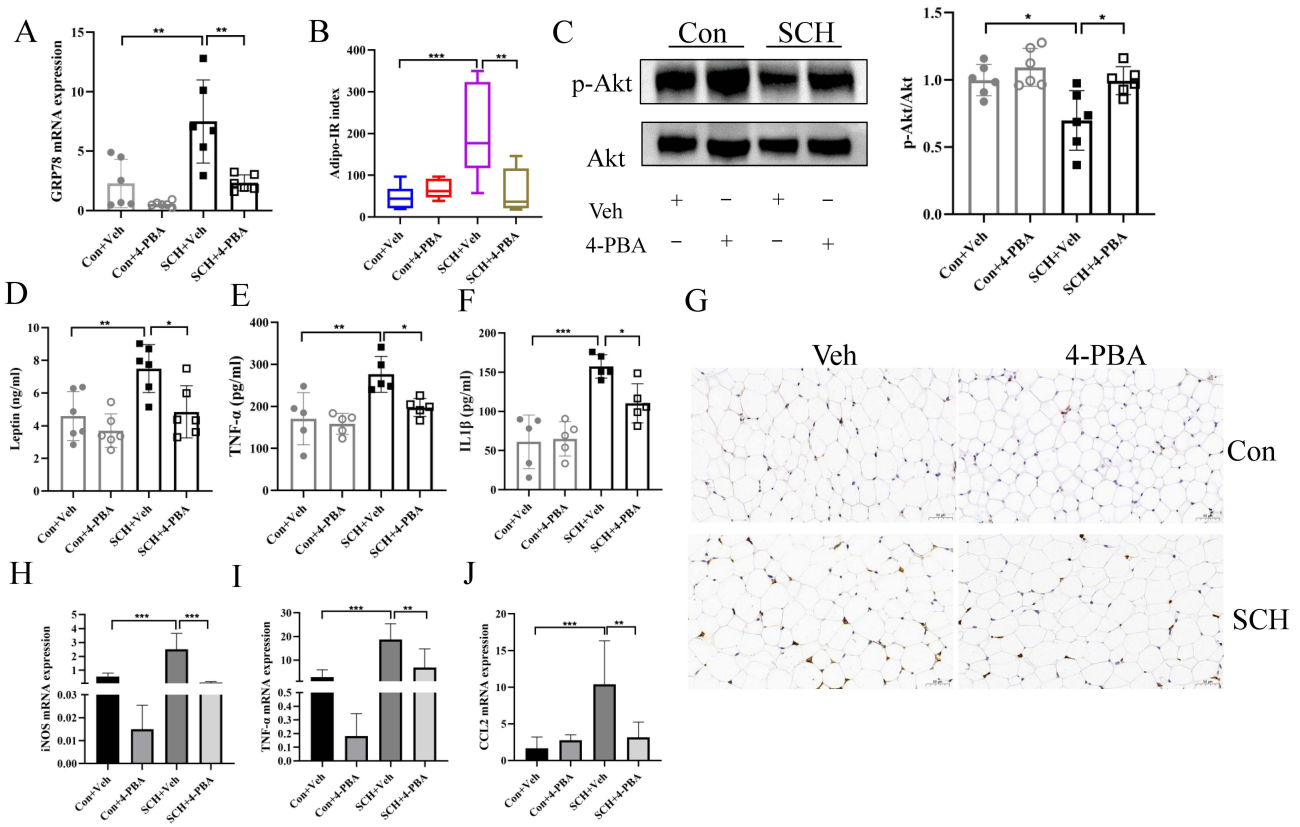

Figure 8 Endoplasmic reticulum stress mediates adipose tissue insulin resistance and M1 macrophage polarization in SCH mice. (**A**) mRNA levels of GRP78 in eWAT. (**B**) Adipo-IR index. (**C**) The expression level of p-Akt/Akt proteins in eWAT was determined by WB. (**D**) Serum concentration of leptin. (**E** and **F**) Serum concentration of TNF-α and IL1β. (**G**) Representative F4/80 immunohistochemistry staining images of eWAT (200×). Scale bars=50μm. (**H–J**) mRNA levels of M1 ATMs markers (iNOS, TNF-α, CCL2) in eWAT. n=5–6. *P < 0.05, **P < 0.01, ***P<0.001.

Abbreviation: GRP78, glucose-regulated protein 78; Adipo-IR, adipose tissue insulin resistance; TNF-α, tumor necrosis factor-α; IL1β, interleukin1β; iNOS, inducible nitric oxide synthase; CCL2, chemokine (C-C motif) ligand 2.

of WAT. NEFA is a byproduct of adipose tissue lipolysis, and the activity of the rate-limiting enzyme that inhibits lipolysis by insulin is reduced in the presence of IR, ultimately leading to elevated NEFA levels. Elevated NEFA levels and Adipo-IR index, as well as decreased p-Akt levels, indicated that SCH mice had a greater adipose tissue IR compared to control. Furthermore, adipocyte hypertrophy, disturbed adipocytokine secretion, and increased inflammatory infiltration are now clearer risk factors for adipose tissue dysfunction,[26,27,36] upon which we clarified that SCH mice had a more severe adipose tissue dysfunction compared to control.

Macrophages are polarized into pro-inflammatory M1 (secreting IL-1β, TNF-α) and anti-inflammatory M2 subtypes, which respectively drive inflammation and promote tissue repair.[37] An adequate balance between M1 and M2 macrophages is conducive to maintaining homeostasis in the tissue internal environment. Furthermore, M1 or M2 macrophage polarization is not a fixed state but a dynamic process which might be reversed under physiological or pathological conditions.[38,39] Up to now, the phenotype of ATMs in SCH mice with elevated TSH levels has not been explored. We observed a significant increase in the infiltration of M1 ATMs in the adipose tissue of SCH mice and confirmed that TSH induced M1 macrophage polarization.

Disruption of the internal homeostasis of the ER by factors such as oxidative stress and ischemia, unfolded proteins accumulate in its lumen, subsequently activating unfolded protein responses (UPRs), which impairs ER function and induces ERS.[40] There is increasing evidence that persistent ERS induces a macrophage polarization imbalance, resulting in an increase in the M1/M2 macrophage ratio, causing chronic inflammation. Inhibiting ERS in adipocytes promotes M2 macrophage polarization, which is critical in treating adipose tissue inflammation.[41,42] To the best of our knowledge, this is the first study to demonstrate that TSH induces ERS in macrophages, which activates the GRP78-ATF6-CHOP

https://doi.org/10.2147/JIR.S522062

signaling pathway. And we intraperitoneally injected mice with 4-PBA to confirm that ERS mediated adipose tissue IR and M1 ATMs polarization in SCH mice.

This study has several limitations that should be acknowledged. First, while the MMI-induced SCH model is commonly employed, its pan-thyroid inhibitory effects may not fully replicate the intricate hormonal regulation observed in humans. Additionally, the findings lack validation in human populations. Future studies should address these gaps by exploring alternative modeling approaches and conducting clinical validation in SCH patients.

In conclusion, the endocrine system, as an important regulatory system, all organs are interconnected and cross-communicate with each other. As an important hormone of the "pituitary-thyroid" axis, TSH may remotely regulates the incidence of adipose tissue IR by modulating the polarization state of ATMs, thus realizing the inter-tissue crosstalk between the "pituitary-thyroid" and "adipose tissue". Our study provide important insights which may support future investigations into the relationship between endocrine organs and metabolic diseases.

Funding

This study was supported by funds from National Natural Science Foundation of China (No.82270832) and Wuhan Science and Technology Bureau Foundation (No.2020020601012214).

Disclosure

All the authors have no conflicts of interest to declare in this work.

References

1. Biondi B, Cappola AR, Cooper DS. Subclinical Hypothyroidism: a Review. *JAMA*. 2019;322(2):153–160. doi:10.1001/jama.2019.9052
2. Maratou E, Hadjidakis DJ, Kollias A, et al. Studies of insulin resistance in patients with clinical and subclinical hypothyroidism. *Eur J Endocrinol*. 2009;160(5):785–790. doi:10.1530/EJE-08-0797
3. Yang W, Jin C, Wang H, et al. Subclinical hypothyroidism increases insulin resistance in normoglycemic people. *Front Endocrinol*. 2023;14:1106968. doi:10.3389/fendo.2023.1106968
4. Baumgartner C, da Costa BR, Collet TH, et al. Thyroid Function Within the Normal Range, Subclinical Hypothyroidism, and the Risk of Atrial Fibrillation. *Circulation*. 2017;136(22):2100–2116. doi:10.1161/CIRCULATIONAHA.117.028753
5. Lee SH, Park SY, Choi CS. Insulin Resistance: from Mechanisms to Therapeutic Strategies. *Diabetes Metab J*. 2022;46(1):15–37. doi:10.4093/dmj.2021.0280
6. Lee YS, Olefsky J. Chronic tissue inflammation and metabolic disease. *Genes Dev*. 2021;35(5–6):307–328. doi:10.1101/gad.346312.120
7. Li H, Meng Y, He S, et al. Macrophages, Chronic Inflammation, and Insulin Resistance. *Cells*. 2022;11(19):3001. doi:10.3390/cells11193001
8. Li Y, Wang L, Zhou L, et al. Thyroid stimulating hormone increases hepatic gluconeogenesis via CRTC2. *Mol Cell Endocrinol*. 2017;446(70):70–80. doi:10.1016/j.mce.2017.02.015
9. Song Y, Xu C, Shao S, et al. Thyroid-stimulating hormone regulates hepatic bile acid homeostasis via SREBP-2/HNF-4alpha/CYP7A1 axis. *J Hepatol*. 2015;62(5):1171–1179. doi:10.1016/j.jhep.2014.12.006
10. Moon MK, Kang GH, Kim HH, et al. Thyroid-stimulating hormone improves insulin sensitivity in skeletal muscle cells via cAMP/PKA/CREB pathway-dependent upregulation of insulin receptor substrate-1 expression. *Mol Cell Endocrinol*. 2016;436(50–8):50–58. doi:10.1016/j.mce.2016.07.018
11. Sarjeant K, Stephens JM. Adipogenesis. *Cold Spring Harb Perspect Biol*. 2012;4(9):a008417. doi:10.1101/cshperspect.a008417
12. Grabner GF, Xie H, Schweiger M, et al. Lipolysis: cellular mechanisms for lipid mobilization from fat stores. *Nat Metab*. 2021;3(11):1445–1465. doi:10.1038/s42255-021-00493-6
13. Chouchani ET, Kajimura S. Metabolic adaptation and maladaptation in adipose tissue. *Nat Metab*. 2019;1(2):189–200. doi:10.1038/s42255-018-0021-8
14. Grant RW, Dixit VD. Adipose tissue as an immunological organ. *Obesity*. 2015;23(3):512–518. doi:10.1002/oby.21003
15. Saklayen MG. The Global Epidemic of the Metabolic Syndrome. *Curr Hypertens Rep*. 2018;20(2):12. doi:10.1007/s11906-018-0812-z
16. Russo L, Lumeng CN. Properties and functions of adipose tissue macrophages in obesity. *Immunology*. 2018;155(4):407–417. doi:10.1111/imm.13002
17. Thomas D, Apovian C. Macrophage functions in lean and obese adipose tissue. *Metabolism*. 2017;72(120–143):120–143. doi:10.1016/j.metabol.2017.04.005
18. Acosta-Martinez M, Cabail MZ. The PI3K/Akt Pathway in Meta-Inflammation. *Int J Mol Sci*. 2022;23(23):15330. doi:10.3390/ijms232315330
19. McNelis JC, Olefsky JM. Macrophages, immunity, and metabolic disease. *Immunity*. 2014;41(1):36–48. doi:10.1016/j.immuni.2014.05.010
20. Orliaguet L, Ejlalmanesh T, Alzaid F. Metabolic and Molecular Mechanisms of Macrophage Polarisation and Adipose Tissue Insulin Resistance. *Int J Mol Sci*. 2020;21(16):5731. doi:10.3390/ijms21165731
21. Nikolajczyk BS, Jagannathan-Bogdan M, Denis GV. The outliers become a stampede as immunometabolism reaches a tipping point. *Immunol Rev*. 2012;249(1):253–275. doi:10.1111/j.1600-065X.2012.01142.x
22. Artyomov MN, Sergushichev A, Schilling JD. Integrating immunometabolism and macrophage diversity. *Semin Immunol*. 2016;28(5):417–424. doi:10.1016/j.smim.2016.10.004

23. Yan Y, Niu Z, Sun C, et al. Hepatic thyroid hormone signalling modulates glucose homeostasis through the regulation of GLP-1 production via bile acid-mediated FXR antagonism. *Nat Commun*. 2022;13(1):6408. doi:10.1038/s41467-022-34258-w
24. Xu C, Zhou L, Wu K, et al. Abnormal Glucose Metabolism and Insulin Resistance Are Induced via the IRE1alpha/XBP-1 Pathway in Subclinical Hypothyroidism. *Front Endocrinol*. 2019;10(303). doi:10.3389/fendo.2019.00303
25. Ying W, Cheruku PS, Bazer FW, et al. Investigation of macrophage polarization using bone marrow derived macrophages. *J Vis Exp*. 2013;76:1. doi:10.3791/50323
26. Longo M, Zatterale F, Naderi J, et al. Adipose Tissue Dysfunction as Determinant of Obesity-Associated Metabolic Complications. *Int J Mol Sci*. 2019;20(9):2358. doi:10.3390/ijms20092358
27. Crewe C, An YA, Scherer PE. The ominous triad of adipose tissue dysfunction: inflammation, fibrosis, and impaired angiogenesis. *J Clin Invest*. 2017;127(1):74–82. doi:10.1172/JCI88883
28. Pellegrinelli V, Carobbio S, Vidal-Puig A. Adipose tissue plasticity: how fat depots respond differently to pathophysiological cues. *Diabetologia*. 2016;59(6):1075–1088. doi:10.1007/s00125-016-3933-4
29. Szkudlinski MW, Fremont V, Ronin C, et al. Thyroid-stimulating hormone and thyroid-stimulating hormone receptor structure-function relationships. *Physiol Rev*. 2002;82(2):473–502. doi:10.1152/physrev.00031.2001
30. Davies T, Marians R, Latif R. The TSH receptor reveals itself. *J Clin Invest*. 2002;110(2):161–164. doi:10.1172/JCI16234
31. Zhang X, Song Y, Feng M, et al. Thyroid-stimulating hormone decreases HMG-CoA reductase phosphorylation via AMP-activated protein kinase in the liver. *J Lipid Res*. 2015;56(5):963–971. doi:10.1194/jlr.M047654
32. Zhang J, Wu H, Ma S, et al. TSH promotes adiposity by inhibiting the browning of white fat. *Adipocyte*. 2020;9(1):264–278. doi:10.1080/21623945.2020.1783101
33. Yang C, He Z, Zhang Q, et al. TSH Activates Macrophage Inflammation by G13- and G15-dependent Pathways. *Endocrinology*. 2021;162(8). doi:10.1210/endocr/bqab077
34. Kahn CR, Wang G, Lee KY. Altered adipose tissue and adipocyte function in the pathogenesis of metabolic syndrome. *J Clin Invest*. 2019;129(10):3990–4000. doi:10.1172/JCI129187
35. Emont MP, Jacobs C, Essene AL, et al. A single-cell atlas of human and mouse white adipose tissue. *Nature*. 2022;603(7903):926–933. doi:10.1038/s41586-022-04518-2
36. Fasshauer M, Bluher M. Adipokines in health and disease. *Trends Pharmacol Sci*. 2015;36(7):461–470. doi:10.1016/j.tips.2015.04.014
37. Liu YC, Zou XB, Chai YF, et al. Macrophage polarization in inflammatory diseases. *Int J Biol Sci*. 2014;10(5):520–529. doi:10.7150/ijbs.8879
38. Tarique AA, Logan J, Thomas E, et al. Phenotypic, functional, and plasticity features of classical and alternatively activated human macrophages. *Am J Respir Cell Mol Biol*. 2015;53(5):676–688. doi:10.1165/rcmb.2015-0012OC
39. Yunna C, Mengru H, Lei W, et al. Macrophage M1/M2 polarization. *Eur J Pharmacol*. 2020;877(173090):173090. doi:10.1016/j.ejphar.2020.173090
40. Saito A, Imaizumi K. Unfolded Protein Response-Dependent Communication and Contact among Endoplasmic Reticulum, Mitochondria, and Plasma Membrane. *Int J Mol Sci*. 2018;19(10):3215. doi:10.3390/ijms19103215
41. Han YB, Tian M, Wang XX, et al. Berberine ameliorates obesity-induced chronic inflammation through suppression of ER stress and promotion of macrophage M2 polarization at least partly via downregulating lncRNA Gomafu. *Int Immunopharmacol*. 2020;86(106741):106741. doi:10.1016/j.intimp.2020.106741
42. Cao W, Zhang T, Feng R, et al. Hoxa5 alleviates obesity-induced chronic inflammation by reducing ER stress and promoting M2 macrophage polarization in mouse adipose tissue. *J Cell Mol Med*. 2019;23(10):7029–7042. doi:10.1111/jcmm.14600